

On the classification and asymptotic behavior of the symmetric capillary surfaces

Zachary Bagley* and Ray Treinen†

August 17, 2016

Abstract

We consider the symmetric solutions to the Young-Laplace equation, and its extensions past vertical points. We provide a classification of all symmetric solutions using certain families of parameters. This classification produces a unified approach to fluid interfaces in capillary tubes, sessile and pendent drops, liquid bridges, as well as exterior and annular capillary surfaces. The generating curves for symmetric solutions have asymptotes for large arclengths, and the behavior of these asymptotes is analyzed.

1 Introduction

The study of the equilibrium shapes of liquids has a long history, though the discovery of the calculus not surprisingly lead to a turning point in these efforts. In 1805 Thomas Young published his celebrated essay [36] followed in 1806 by a more mathematical treatment by Pierre-Simon Laplace [19], establishing the Young-Laplace equation

$$\nabla \cdot \left(\frac{\nabla u}{\sqrt{1 + |\nabla u|^2}} \right) = \kappa u + \lambda, \quad (1)$$

where the left hand side is the mean curvature operator, $2H$, u is the height of the fluid interface, $\kappa = \rho g / \sigma$, ρ is the density of the fluid, σ is the surface tension of the fluid interface, g is a gravitational constant, and λ is a Lagrange multiplier that is used if volume constraints are considered. Solutions of this equation are called capillary surfaces. In 1830 Gauss [13] obtained the same results using the method of virtual variations and at the same time establishing natural boundary conditions for the physical problem of determining the height of the fluid interface in a container. Much has transpired in the last two centuries, and the current standard reference is a manuscript by Finn [8].

In this paper, we will investigate the symmetric solutions of (1), and their extensions past vertical points. The symmetric solutions can be described by a generating curve, and we will

*Department of Mathematics, Texas State University, 601 University Drive, San Marcos, Texas 78666 (zaba6933@colorado.edu).

†Department of Mathematics, Texas State University, 601 University Drive, San Marcos, Texas 78666 (rt30@txstate.edu).

choose a form of (1) that is in terms of arclength. That generating curve will depend on certain parameters which we will describe. The main physical distinction between surfaces is that some are simply connected, and others are topologically annular. In particular, we will provide a classification scheme for all symmetric solutions to the Young-Laplace equation in terms of these parameters, and we will also analyze the asymptotic behavior of all of these solutions for large arclength.

There are many problems where one may prove that solutions to (1) are necessarily symmetric about a vertical axis. See Gonzalez [15] and Wentz [34] for examples of this. Another approach is to prove existence of solutions under the assumption of symmetry, and then to quote a uniqueness theorem, say as might be found in [8].

Further, frequently treatments of symmetric capillary problems in the last half-century have been restricted to simply connected domains, or geometric problems which admit a solution which is topologically equivalent to a disc. We are aware of three types of problems that deviate from this trend. First is the study of liquid bridges, for which see work by Athanassenas [1], Finn and Vogel [11] and Vogel [33] for example. Next are exterior problems such as a rod dipped into an unbounded sea of liquid, as can be found in Johnson and Perko [18], Siegel [25], Turkington [31], and Vogel [32]. Finally, there are applications involving multiple fluids or particles floating on the fluid interface. For the third type we do not yet know if the configurations are symmetric, but nevertheless we are able to obtain some results under the assumption of symmetry. The one exception that the authors are aware of is a proof of a symmetry property for three immiscible fluids by Treinen [30]. Some examples involving multiple fluids or particles floating on the fluid interface are papers by Elcrat, Neel and Siegel [6], Elcrat and Treinen [7], Finn [9], Finn and Sloss [10], Finn and Vogel [12], McCuan [21], McCuan and Treinen [22, 23], and Treinen [28]. Given this interest in problems of annular type (possibly unbounded), or applications that use them, this leads to a study motivated by that perspective. See Elcrat, Kim and Treinen [5], Gordan and Siegel [16, 17], Siegel [26], and Treinen [29].

2 Initial exploration and classification

It is our goal to provide a framework to classify all symmetric solutions of the Young-Laplace equations. Our methods are numerical in nature, and as such may be seen as conjectural, though we have taken extreme steps in reducing errors to the limits of what is currently computationally feasible. We begin this process by considering some illustrative examples.

We assume the surface is symmetric about the vertical axis, and thus has a generating curve. To determine this, we use the form of the differential equation parameterized by arclength s which is given by the following system:

$$\frac{dr}{ds} = \cos \psi \tag{2}$$

$$\frac{du}{ds} = \sin \psi \tag{3}$$

$$\frac{d\psi}{ds} = \kappa u - \frac{\sin \psi}{r}. \tag{4}$$

Here r is the radius, u is the height above the r -axis, and ψ is the inclination angle. We have

normalized so that the Lagrange multiplier λ is zero. The solution to this system may be extended past both vertical points and inflection points, which we now turn to illustrate.

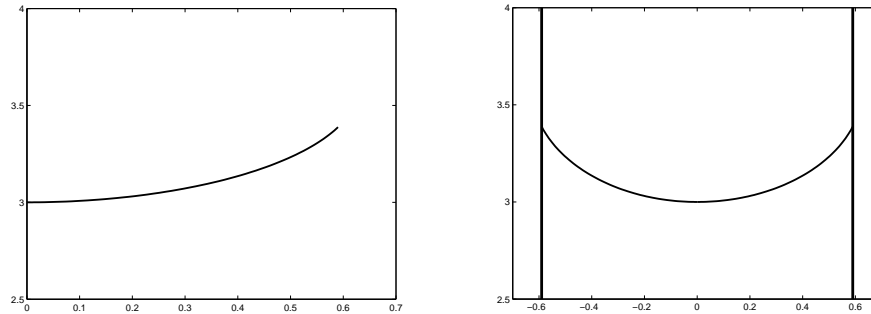


Figure 1: Generating curve for a capillary tube (L), and the interface it represents in a capillary tube, with the fluid below the interface (section shown) (R).

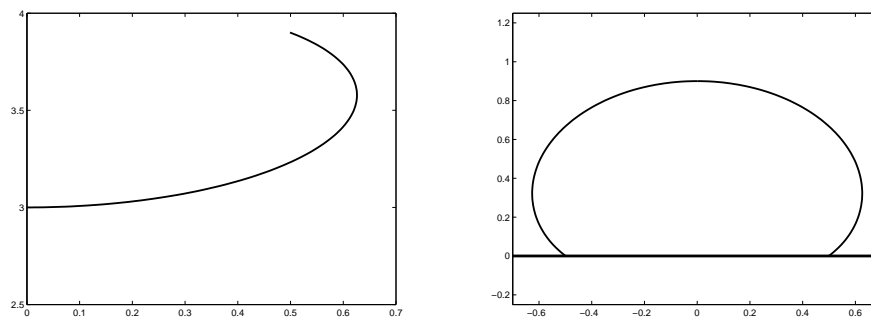


Figure 2: Generating curves for a sessile drop (L), and that sessile drop (section shown) (R).

Our first example is a solution to the system (2)-(4) so that the ending inclination angle ψ attains a value $\pi/2 - \gamma$ at a prescribed radius r where γ is a contact angle with a cylindrical wall at r . This is a generating curve for the classical capillary tube, and both the generating curve and the capillary tube are shown in Figure 1. Our next example is solution of the system so that the ending inclination angle ψ attains a value $\pi - \gamma$ when the enclosed volume attains a prescribed value. This forms a generating curve that when inverted and vertically translated (using Lagrange multipliers) describes a sessile drop, as is shown in Figure 2. Both this example and the previous one are attained by using the initial conditions $r(0) = 0$, $u(0) = u_0$, and $\psi(0) = 0$, and then finding the value of u_0 that satisfies the above conditions. We have chosen to illustrate both of these with a value of $u_0 = 3$. Then, if we continue the solution, it extends past a point of self intersection and becomes immersed. See Figure 3 (L). For physical problems involving fluid interfaces, we may only use portions of the curve that are embedded, as in Figure 3 (R). By doing so we pick up some types of annular capillary surfaces, and also components that may be used to construct liquid bridges. If we continue the solution for much

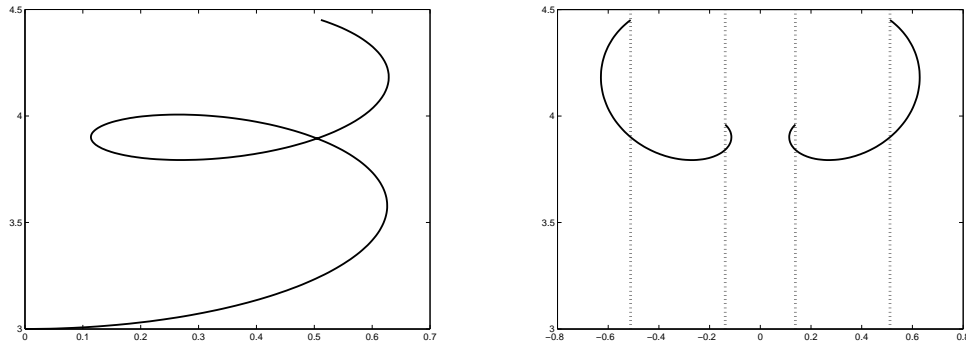


Figure 3: Immersed solutions (L), and the corresponding annular capillary surface (section shown) (R). Here we have chosen to illustrate an annular capillary surface that contains vertical points, and extends beyond the radii of the endpoints for the generating curve.

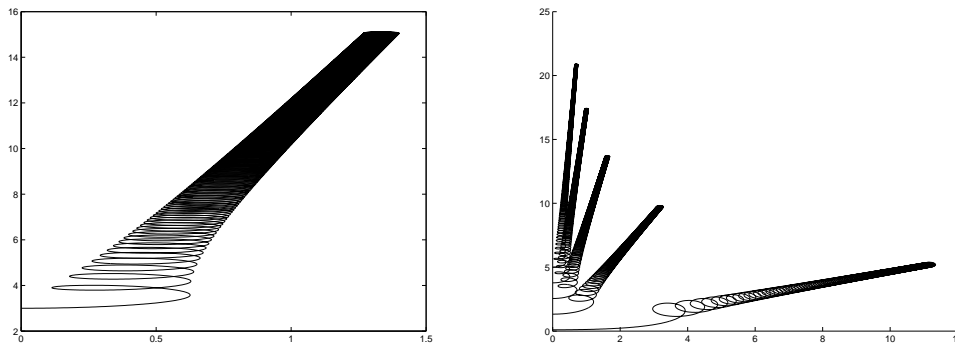


Figure 4: The large arclength extension of the immersed solution (L), and family of generating curves (R).

larger arclength, we begin to see the asymptotic behavior, as seen in Figure 4 (L).

Upon changing the initial height, we find a family of solutions. It is apparent that the solutions to the system are asymptotic to lines in the ru -plane, and that the slope of each linear asymptote is dependent on the initial value u_0 . Five different choices of initial heights u_0 are shown in Figure 4 (R).

Pendent drops may be described by the system (2)-(4) with κ replaced by $-\kappa$, and our next step is to make the connection between the above and pendent drops. Take a selection of generating curves from the last example, and at each starting point replace the initial angle ψ with $-\pi$. This will pair an inverted pendent drop with each immersed solution achieved above. Upon reflection this curve is in its traditional orientation. In Figure 5 we show the generating curve and the corresponding pendent drop hanging from a circular tube. See Figure 6 for a comparison with pendent drops where the left figure has been described by our framework, and the right figure is a reflected view without the immersed portions. Concus and Finn [4] wrote

pioneering work in this connection.

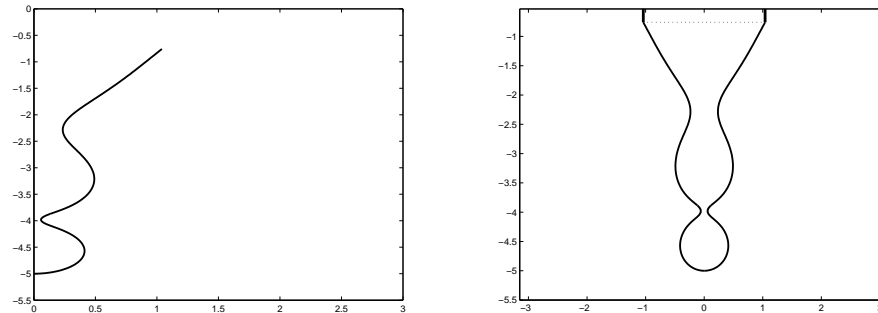


Figure 5: Generating curve for a pendent drop (L), and that pendent drop suspended from a circular tube (section shown) (R).

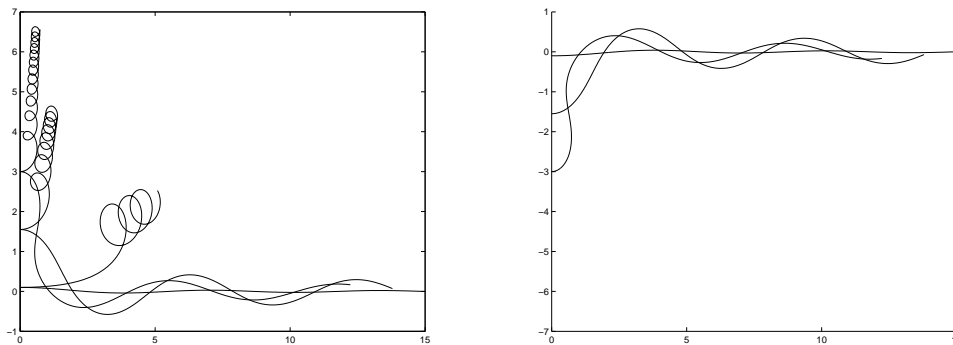


Figure 6: Connections to pendent drops.

Consider again the immersed portions of the generating curve. A question is if we have attained all possible annular capillary surfaces with the family generated by the initial conditions $r(0) = 0, u(0) = u_0, \psi(0) = 0$ with $u_0 \in \mathbb{R}$? We have an immediate negative answer. Start with a horizontal point at $r_0 = 0.5$ and $u_0 = 3$, and then extend in both directions as in Figure 7. The curve does not extend to $r = 0$. We will provide more detail for the difference between these two types of solution curves in Section 7. For the moment we merely remark that it is a fact that the inclination angle ψ must be 0 at $r = 0$ due to the symmetry of the problem and the regularity theory, say as might be extended from work of Giusti [14]. One implication is that we have a way to parameterize this new family of annular capillary surfaces. If we consider the point on the generating curve that is closest to the vertical axis, we may denote this point as (r_0, u_0) and conclude by elementary calculus that $\psi_0 = -\pi/2 + n\pi$ there for some $n \in \mathbb{Z}$. It is possible to normalize so that $\psi_0 = -\pi/2$. Thus we have established a two-parameter family parameterized by (r_0, u_0) with $\psi_0 = -\pi/2$ that is distinct from the family generated by $(0, u_0)$ with $\psi(0) = 0$.

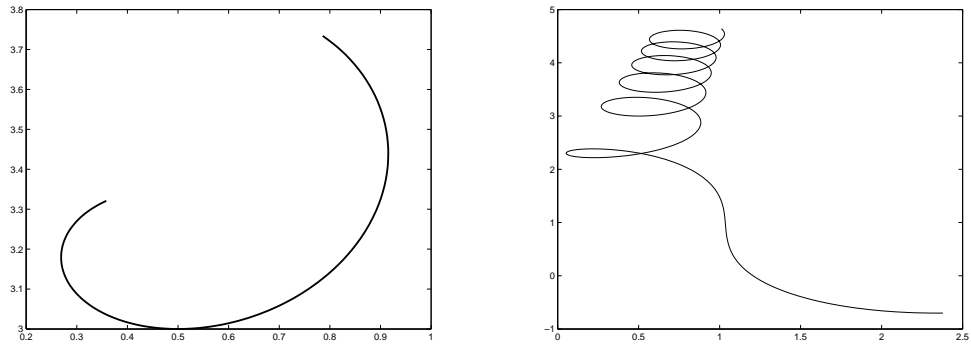


Figure 7: An example of annular capillary surfaces that do not touch the vertical axis.

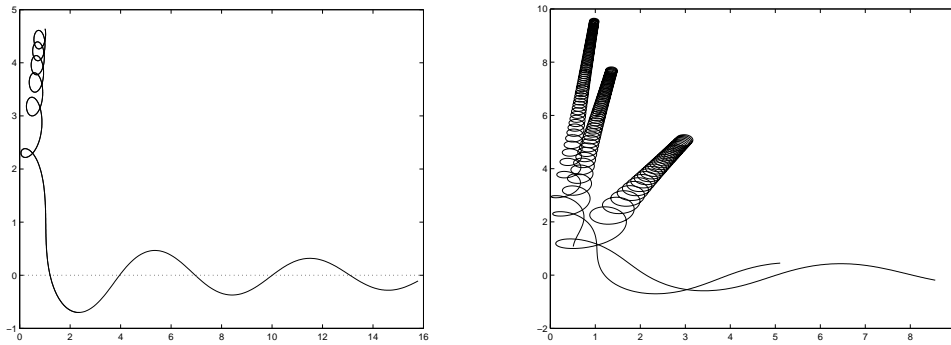


Figure 8: Oscillation about the r -axis (L) and three members of the family parametrized by (r_0, u_0) .

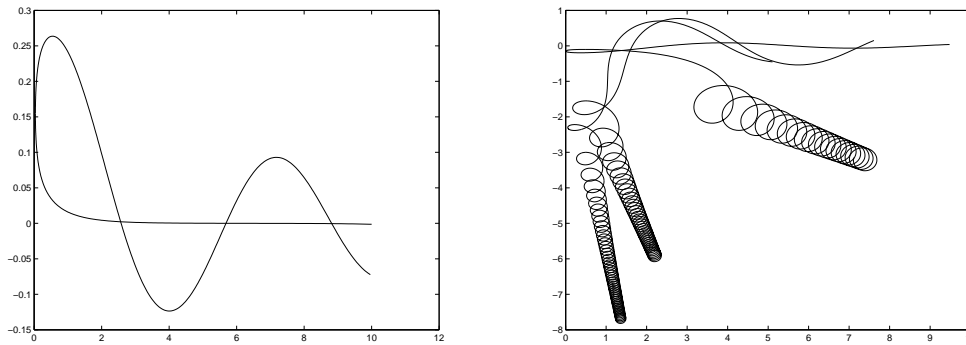


Figure 9: A special case with exponential decay (L) and three members of the family parametrized by (r_0, u_0) with $u_0 < 0$ (R).

Consider the right graph in Figure 7, and in particular the portion of the curve that extends down and towards the r -axis. If you remove the upper immersed part of this curve, then this is an example of an inverted annular pendent drop. To the extent of the authors' knowledge, this is the first explicit example given of a capillary surface of this type in the literature. As this appears to be the case, we include a brief exploration of the subject in Section 3.

It should be noted that the same type of oscillation about the r -axis that occurs for the pendent drops also occurs for the annular pendent drops, as is shown in Figure 8 (L). A good reference for the classical behavior is [8].

In our final examples we consider a few different values of u_0 in this two-parameter family. The right graph of Figure 8 contains three examples where $u_0 > 0$. The same type of linear asymptotics is apparent, and the slope of these asymptotes also changes with the generating parameters. The right graph of Figure 9 contains three examples of $u_0 < 0$, which has similar behavior. In particular in both of these examples it should be pointed out that the first embedded portion lengthens as u_0 becomes smaller in magnitude, here we mean the portion of the generating curve from $-\pi/2 \leq \psi \leq \pi/2$ in the case when $u_0 > 0$. This fact was proved in [5]. In this way one may see that the unbounded liquid bridge fits into this classification scheme as $u_0 \rightarrow T(r_0)$ where the function T is defined to precisely give this curve with exponential decay. See Siegel [25], Turkington [31], and Vogel [32] for discussions of this behavior, shown in Figure 9 (L).

We claim that the only remaining symmetric capillary surface is the singular solution, which can be seen as a point-wise limit of pendent drops as $u_0 \rightarrow -\infty$. Where, of course κ is replaced by $-\kappa$. See Concus and Finn [2, 3] and Nikolov [24]. This discussion leads to the following conjecture, which we state as a conjecture, though the contents of this paper give strong numerical evidence supporting it.

Conjecture 2.1 *Let H be the mean curvature operator, and let κ be either a positive or negative real number. Let \mathcal{U} be a solution of*

$$2H = \kappa u \tag{5}$$

that is symmetric about the vertical axis. Then, using

$$\frac{dr}{ds} = \cos \psi \tag{6}$$

$$\frac{du}{ds} = \sin \psi \tag{7}$$

$$\frac{d\psi}{ds} = \kappa u - \frac{\sin \psi}{r} \tag{8}$$

with

$$r(0) = r_0 \tag{9}$$

$$u(0) = u_0 \tag{10}$$

$$\psi(0) = \psi_0, \tag{11}$$

\mathcal{U} can be represented in one of the following ways:

1. $r_0 = 0$, $\psi_0 = 0$, $u_0 \in \mathbb{R}$ and \mathcal{U} is described by some interval of arclength $s_0 \leq s \leq s_1$. If $\kappa < 0$, then the representation is traditionally reflected about the r axis,
2. $r_0 > 0$, $\psi_0 = -\pi/2$, $u_0 \in \mathbb{R}$ and \mathcal{U} is described by some interval of arclength $s_0 \leq s \leq s_1$. If $\kappa < 0$, then the representation is traditionally reflected about the r axis,
3. \mathcal{U} is the singular solution.

All of the simply connected capillary surfaces are contained in Case 1, as well as some of the annular capillary surfaces. Case 2 contains the unbounded liquid bridge where $u_0 = T(r_0)$ with $s_1 = \infty$ and, barring the singular solution, Case 2 also contains the remaining surfaces that are not simply connected, which as we will see in Section 7 is the bulk of the surfaces of this type.

3 Annular Pendent Drops

As we stated above, pendent drops may be described by the system (2)-(4) with κ replaced by $-\kappa$. Geometrically this is a reflection of the curve about the r -axis, or it could be seen as changing the orientation of the gravitational potential. We note that perhaps the easiest way to formulate the problem is as either an annular hanging tube attached to a larger volume of fluid, or as a pipet with an annular opening and with fixed pressure. Wente [35] considered the simply connected version of these two problems, as well as that of a drop hanging from a horizontal plate. It follows from the symmetry results proved by Wente [34] that any attempt at constructing an annular analogue of the drop hanging from a single horizontal plate will lead to a more classical simply connected pendent drop. Of course, one may attempt to rectify this by considering a system of plates at different heights, but we note that the heights of the plates would depend on the contact angles and the enclosed volume, and thus with the exception of some rare cases, the solution would not be symmetric about the vertical axis, even if the supporting configuration is. It is unfortunately outside of the scope of this paper to perform a detailed analysis of these surfaces.

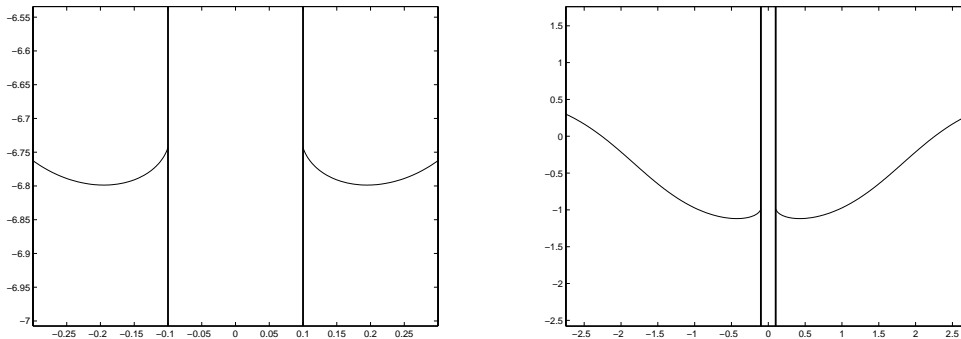


Figure 10: Two examples of annular pendent drops, where the fluid is above the interface.

The two configurations that we are able to formulate, that of the annular hanging tube, and that of the “medicine dropper” with annular opening both have the same boundary value

problem. As in [35], we expect that these two different formulations will have different stability properties even though they both satisfy the same boundary value problem. The system (2)-(4) with κ replaced by $-\kappa$ is given the boundary values of

$$\psi_a = \frac{\pi}{2} - \gamma_a \quad (12)$$

$$\psi_b = \gamma_b - \frac{\pi}{2} \quad (13)$$

where the physical contact angles γ_a and γ_b are measured interior to the liquid at radii a and b , respectively. We give two numerical examples. In Figure 10 we consider contact angles $\gamma_a = 0.9\pi$ and $\gamma_b = 0.7\pi$. On the left $a = 0.1$ and $b = 0.3$, while on the right $a = 0.1$ and $b = 1.75$. Notice that the scales vary between plots, while a remains fixed.

4 Power Series Expansion

So far we have not addressed the singularity at $r = 0$. We do so here with a degree of accuracy that is sufficient to achieve error on the order of machine epsilon using the Runge-Kutta-Felberg implementation ODE45 in Matlab.

We computed the power series expansion of the solution centered at the arclength $s = 0$ up to s^6 terms, and the result is collected in the following theorem. While lengthy, the computation is straightforward. Lohnstein [20] and Wente [35] also produced related calculations.

Theorem 4.1 *The solution of (2)-(4) with $r_0 = 0$ and $\psi_0 = 0$ is given by*

$$\begin{aligned} r &\approx s - \frac{\kappa^2 u_0^2}{24} s^3 - \frac{\kappa^3 u_0^2}{160} s^5, \\ u &\approx u_0 + \frac{\kappa u_0}{4} s^2 + \left(\frac{\kappa^2 u_0}{64} - \frac{\kappa^3 u_0^3}{192} \right) s^4, \\ &\quad + \left(\frac{\kappa^3 u_0}{2,304} - \frac{\kappa^4 u_0^3}{720} - \frac{\kappa^5 u_0^5}{138,240} \right) s^6, \\ \psi &\approx \frac{\kappa u_0}{2} s + \frac{\kappa^2 u_0}{16} s^3 + \left(\frac{\kappa^3 u_0}{384} - \frac{\kappa^4 u_0^3}{1,920} - \frac{\kappa^5 u_0^5}{23,040} \right) s^5. \end{aligned}$$

through 6th degree terms.

We used this to determine an arclength $s = s^*$ where if $0 \leq s \leq s^*$ we use

$$\begin{aligned} \frac{dr}{ds} &\approx 1 - \frac{\kappa^2 u_0^2}{8} s^2 - \frac{\kappa^3 u_0^2}{32} s^4, \\ \frac{du}{ds} &\approx \frac{\kappa u_0}{2} s + \left(\frac{\kappa^2 u_0}{16} - \frac{\kappa^3 u_0^3}{48} \right) s^3 + \left(\frac{\kappa^3 u_0}{384} - \frac{\kappa^4 u_0^3}{120} - \frac{\kappa^5 u_0^5}{23,040} \right) s^5, \\ \frac{d\psi}{ds} &\approx \frac{\kappa u_0}{2} + \frac{3\kappa^2 u_0}{16} s^2 + \left(\frac{5\kappa^3 u_0}{384} - \frac{\kappa^4 u_0^3}{384} - \frac{\kappa^5 u_0^5}{4,608} \right) s^4 \end{aligned}$$

and otherwise we use (2)-(4).

Here s^* is chosen so that for the range of u_0 values used produces an error at s^* comparable with machine ϵ . Thus we have minimized the error in using ODE45. For large arclength, computations are intensive, and outstrip reasonable use of a single workstation. We use ODE45 to compute the data $\{r_0, r_1, \dots, r_n\}$ and $\{u_0, u_1, \dots, u_n\}$ as approximation to the continuous solution. Here n is the index associated with $s_n = \ell$, which is some large ending arclength. In what follows we will use $\ell = 20,000$.

5 Least Squares using the SVD

We will use least squares to determine the regression line for the data $\{r_0, r_1, \dots, r_k\}$ and $\{u_0, u_1, \dots, u_k\}$ for some large k . As we will see in Sections 6 and 8, this is used to approximate the linear asymptote of the data. We will use the singular value decomposition to compute this regression line as follows.

Given $A \in \mathbf{R}^{m \times n}$, we have

$$V = [\mathbf{v}_1 | \mathbf{v}_2 | \dots | \mathbf{v}_n] \in \mathbf{R}^{n \times n},$$

and

$$U = [\mathbf{u}_1 | \mathbf{u}_2 | \dots | \mathbf{u}_n] \in \mathbf{R}^{m \times m}$$

both with orthonormal columns, and $\Sigma \in \mathbf{R}^{m \times n}$ is diagonal and has nonincreasing positive entries σ_j , so that $A\mathbf{v}_j = \sigma_j\mathbf{u}_j$, $1 \leq j \leq n$. The index of the smallest positive singular value gives the rank of A , and we denote it by p . The Reduced Singular Value Decomposition (SVD) is

$$A = \hat{U}\hat{\Sigma}\hat{V}^*$$

where the columns of U , Σ , and V are used only when they are needed to reconstruct A , and these reduced matrices are given $\hat{\cdot}$ notation. Here $\hat{U} \in \mathbf{R}^{m \times p}$, $\hat{\Sigma} \in \mathbf{R}^{p \times p}$, and $\hat{V}^* \in \mathbf{R}^{p \times n}$.

We obtain data $\{r_0, r_1, \dots, r_k\}$ and $\{u_0, u_1, \dots, u_k\}$ that corresponds to coordinates along a given approximate solution curve. The least squares line $y = c_1r + c_0$ best satisfies

$$A\mathbf{c} := \begin{bmatrix} 1 & r_0 \\ 1 & r_1 \\ \vdots & \vdots \\ 1 & r_k \end{bmatrix} \begin{bmatrix} c_0 \\ c_1 \end{bmatrix} = \begin{bmatrix} u_0 \\ u_1 \\ \vdots \\ u_k \end{bmatrix} =: \mathbf{u}. \quad (14)$$

First, compute $A = \hat{U}\hat{\Sigma}\hat{V}^*$, then the orthogonal projector $P = \hat{U}\hat{U}^*$ projects onto the range of A , giving $\mathbf{y} = P\mathbf{u} = \hat{U}\hat{U}^*\mathbf{u}$. The algorithm is

1. Compute $A = \hat{U}\hat{\Sigma}\hat{V}^*$.
2. Compute $\hat{U}^*\mathbf{u}$.
3. Solve the diagonal system $\hat{\Sigma}\mathbf{w} = \hat{U}^*\mathbf{u}$ for \mathbf{w} .
4. Set $\mathbf{c} = \hat{V}\mathbf{w}$.

See Trefethen and Bau [27] for an excellent exposition of the merits of this choice of least squares method.

6 Asymptotic Behavior for $r_0 = 0$

In what follows, we determine the asymptotic behavior of the solutions to the capillary equations, and we begin with the case where $r_0 = 0$. Given an initial height u_0 , we have computed approximations to the solution curve, as given by the data $\{r_0, r_1, \dots, r_n\}$ and $\{u_0, u_1, \dots, u_n\}$ with a large ending arclength ℓ , and n is the index such that the arclength $s_n = \ell$. First note that the least squares line for the data $\{r_0, r_1, \dots, r_n\}$ and $\{u_0, u_1, \dots, u_n\}$ remains between the upper and lower envelopes generated by each individual solution. Then we note that Elcrat, Kim, and Treinen [5] and Treinen [29] proved that for any symmetric annular capillary surface the distance between the left vertical point and the right vertical point go to zero as the height of the horizontal point between them goes to infinity. It follows that the least squares line will converge to the asymptote in some sense, provided that asymptote is linear. As further evidence that the data has a linear asymptote, see Figure 11, which shows a small range of u_0 values in the family of generating curves that start on the u -axis, and their corresponding regression lines as computed using the methods of Section 5. Then a natural question to ask is what the slope and intercept of these regression lines are, in terms of the initial height u_0 .

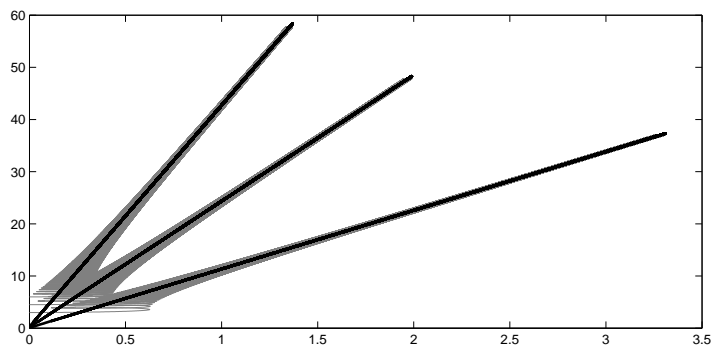


Figure 11: Three of the regression lines we computed shown with the corresponding data.

In Figure 12 (L) we see that the intercept of the regression line starts out near zero, and slowly increases. Over the interval we computed it, it increases to a value of 1.2 when $u_0 = 32$. Given the nature of approximation in obtaining our data for the generating curve, we suggest that this could be error from the combination of methods used. If so, and we take a normalized value to be the intercept values divided by u_0 , then we find the normalized value is approximately 0.0375. To be clear, the findings of our simulations strongly suggest that the intercept of the asymptote is 0. This will be supported further in Section 8.

In Figure 12 (R) we graph slope of the least squares lines over u_0 in the range $[0, 32]$. Our initial results indicated that the slope of the asymptote was a quadratic curve, though, as we will see it is not quite so simple. This led to a much more accurate numerical exploration, with the prescribed error on the order of machine epsilon. In order to be more precise, we assume that the slope is of the form x^α , then in Figure 13 we plot α with u_0 first in the range $[0, 0.3]$, and again in the range $[10, 52]$. We then see that for small u_0 values the power of the slope is close to $1/3$, and for large u_0 values the slope of the regression line is not quite u_0^2 , but close,

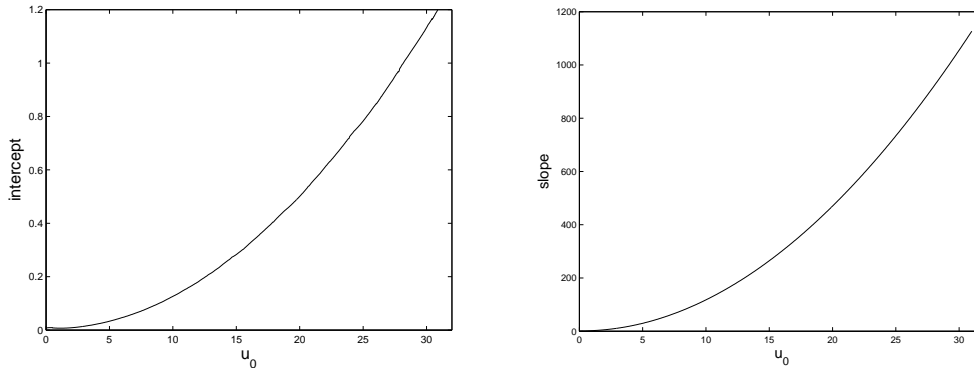


Figure 12: The intercept (L) and slope (R) of the regression line as a function of u_0 .

and as $u_0 \rightarrow \infty$, the evidence strongly suggests that $\alpha \rightarrow 2$.

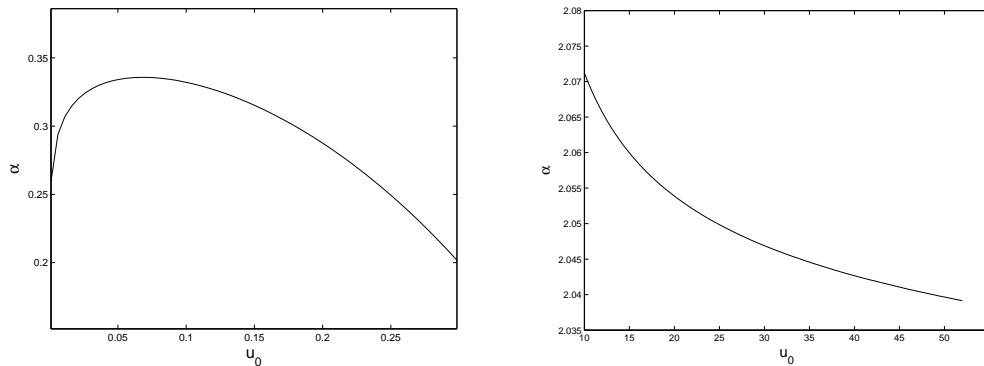


Figure 13: Graphs of the power α under the assumption that the slope is of the form x^α . Small u_0 values are on the left, and larger u_0 values are on the right.

Given the supporting evidence, it is reasonable to assume that the asymptotic behavior is linear. After the error in estimating the solution to the initial value problem, the second type of error is the difference between the least squares line and the asymptotic line. To counter this we take rather large values of ending arclength ℓ , and as we have mentioned before, we find $\ell = 20,000$ to be sufficient. As we discussed earlier, the loops get smaller when any horizontal point $(r_0, u_0) \rightarrow (\infty, \infty)$. The least squares line does not leave the envelope generated by the solution curve, thus the least squares line approaches the asymptotic line as $\ell \rightarrow \infty$. As for the convergence of these quantities as the arclength gets longer, Figure 14 illustrates that the partial arclength values of both the intercept the power α as functions of u_0 are Cauchy sequences in the sense that they are approaching a limiting function of u_0 as $\ell \rightarrow \infty$. The relatively small range of u_0 was chosen to highlight this feature, and to dampen any changes of the limiting functions over a longer range of u_0 .

The above numerical evidence supports the following.

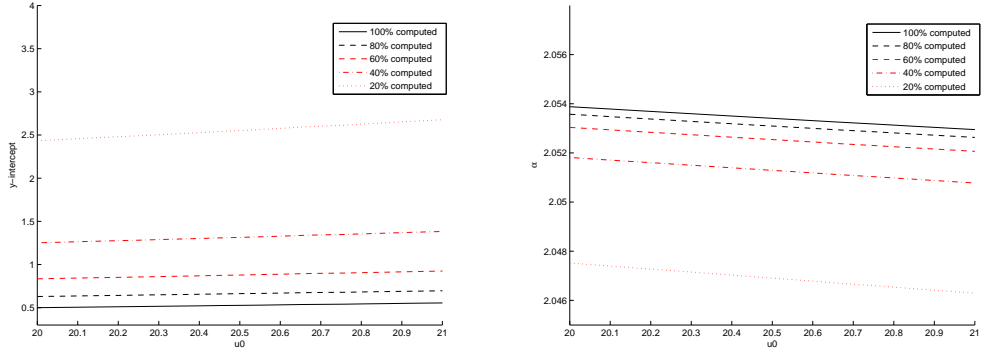


Figure 14: Convergence of the intercept as the ending arclength $\ell \rightarrow \infty$ (L), and the convergence of the power α as the ending arclength $\ell \rightarrow \infty$ (R).

Conjecture 6.1 *Solutions of the system*

$$\frac{dr}{ds} = \cos \psi \tag{15}$$

$$\frac{du}{ds} = \sin \psi \tag{16}$$

$$\frac{d\psi}{ds} = \kappa u - \frac{\sin \psi}{r} \tag{17}$$

with

$$r(0) = 0 \tag{18}$$

$$u(0) = u_0 \tag{19}$$

$$\psi(0) = 0, \tag{20}$$

have linear asymptotes as $s \rightarrow \infty$. The linear asymptotes pass through the origin. Further, the slopes of the linear asymptotes depend on u_0 , and that dependence is approximately quadratic if u_0 is sufficiently far from 0. As $u_0 \rightarrow \infty$, the slope of the asymptote converges to a line with slope u_0^2 . For u_0 small enough, the slope has the form x^α with α between $1/4$ and $1/3$.

7 A parameter space for annular capillary surfaces with $r_0 > 0$

Considering the implication of Figure 7, in that we have symmetric capillary surfaces that do not fit in the family parametrized by u_0 with $r_0 = 0$, we are then left with a secondary two dimensional parameter space of (r_0, u_0) for $r_0 > 0$. We normalize this parameter space so that $\psi = -\pi/2$ at this vertical point along that curve that is nearest to the vertical axis. While we discussed this in leading up to Conjecture 2.1, it remains to give some way to determine the difference between the two types of parametrization. In Figure 15 (L) we see that curves from two different parametrization families can become nearly indistinguishable somewhere along

their trajectories. Two questions arise. First, how can one know if their normalized (r_0, u_0) point is truly the furthest point to the left along the trajectory of the curve? Second, how do we know if we actually have a candidate for a (r_0, u_0) vertical point? We are able to address both of these questions while at the same time reducing the size of the parametrization space substantially.

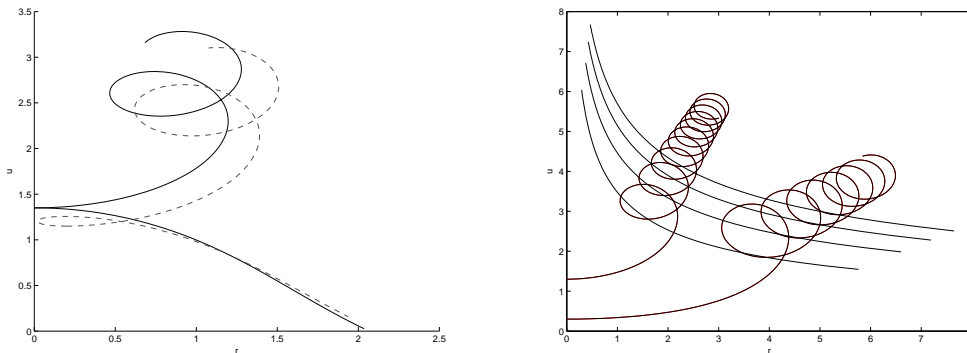


Figure 15: Two nearby curves of both types (L), the first four curves of horizontal points with example generating capillary curves where $r_0 = 0$ (R).

To begin, let $r_0 = 0$ and $u_0 > 0$. Define $f_1 = \langle r, u \rangle$ by the assignment $u_0 \mapsto \langle r_\pi, u_\pi \rangle$ where the inclination angle ψ of the generating curve is π at that point. Thus we see f_1 is a curve made up of the first horizontal points along the generating curves in the family of solutions for $r_0 = 0$ and $u_0 > 0$. Figure 15 (R) shows two example curves from the family of solution curves where $r_0 = 0$. Also shown there are four curves made up of further horizontal points generated by these capillary curves for $u_0 \in (0, \infty)$. There are infinitely many more of these curves of horizontal points, of course, but in fact we will only need the first of these. We define these curves so that for $i = 2, 3, \dots$, f_i is determined by $u_0 \mapsto \langle r_{i\pi}, u_{i\pi} \rangle$. If we start a capillary curve with a horizontal point in this first region between the coordinate axes and f_1 , then we find that the next horizontal point of this capillary curve appears between f_1 and f_2 . The further horizontal points of that capillary curve are interleaved between the f_i , for $i = 2, 3, \dots$.

Next, we would like to see if that region bounded by the coordinate axes and f_1 is sufficient to parametrize the entire family of generating curves. Figure 16 (L) shows the horizontal points generated by a grid of horizontal points started between f_1 and f_2 . In all cases there are resulting points contained in the region bounded by f_1 and the coordinate axes. As the curve f_1 is approached, the horizontal points converge to the vertical axis. There is some error, but given our starting point, we are unable to account for the singularity in the system of differential equations in any reasonable way. Thus this error is to be expected. We see this error most dramatically near the origin.

Then, as the normalized vertical point of a capillary curve is to the left of its first horizontal point, we have restricted the unbounded parameter space into a significantly smaller parameter space, though still unbounded, as f_1 is asymptotic to both the axes.

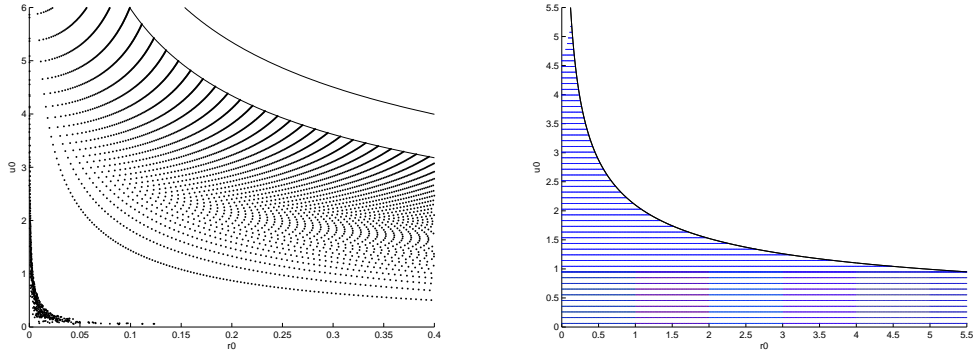


Figure 16: Evidence that the unbounded region between the axes and the first curve of horizontal points generates all cases where $r_0 > 0$ (L), all the cases of initial values where we generated solution curves, and their corresponding regression lines (R).

8 Asymptotic Behavior for $r_0 > 0$

Finally, we will analyze the asymptotic behavior of capillary curves that are in the region between the coordinate axes and f_1 . As before, we have obtained extremely accurate results for computations over large arclengths from weeks of parallel processing on the STAR cluster at Texas State University. The resulting data is generated at approximately 9000 gridpoints, and uses approximately 1TB of storage space. The region we obtained results for is shown in Figure 16 (R). Again, we were able to use the SVD based least squares algorithm to analyze this data, and a prototype is shown in Figure 17 (L).

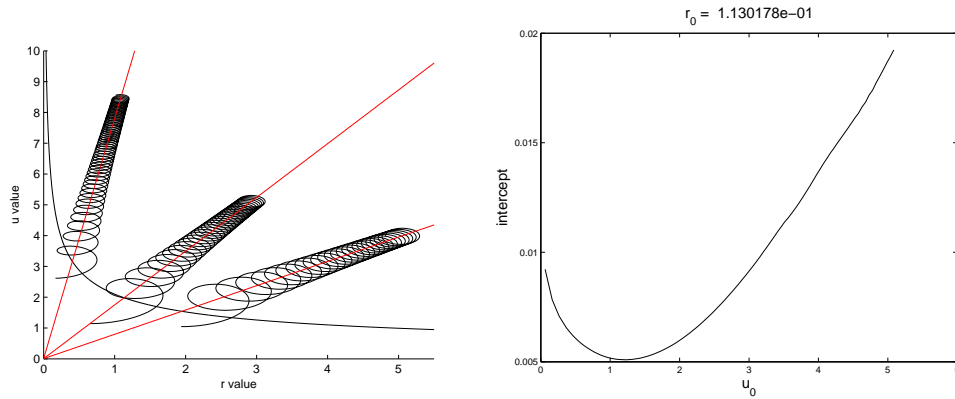


Figure 17: Prototype regression lines for three capillary curves in the reduced parameter space (L). The intercept as a function of u_0 with a fixed $r_0 = 0.11302$. Notice that the intercept is approximately 0 (R).

As a way of summarizing the rather large data set that we have generated, we will look at a 100 by 100 grid of (r_0, u_0) values. The data we generated is not uniformly spaced, with the

largest shift in the grid occurring around $u_0 \approx 0.94$. We use a non-structured interpolation which is of class C^1 except at data points. The information that we interpolate is the vertical intercept and the slope of the least squares lines, and further under the assumption that the slope is of the form x^α , we interpolate the power α as well.

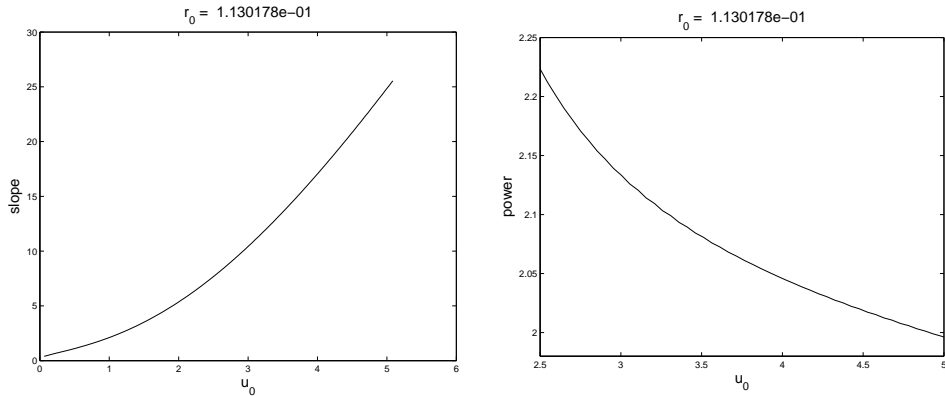


Figure 18: The slope as a function of u_0 with a fixed $r_0 = 0.11302$ (L). A magnified plot of the power α under the assumption that the slope is of the form x^α , with magnification centered on the largest values of u_0 in this range, and $\alpha \rightarrow 2$ (R).

We first present this information as a sample of three r_0 values that are representative of small, medium, and large values. Then we take all of the u_0 values in our interpolating grid that correspond to that sample r_0 , and we plot the intercept, slope, and power as a function of u_0 given that choice of r_0 . This is collected in Figures 17 (R) and 18-22. In all of these examples, the intercept is approximately 0, and this is a good representation of the data we generated.

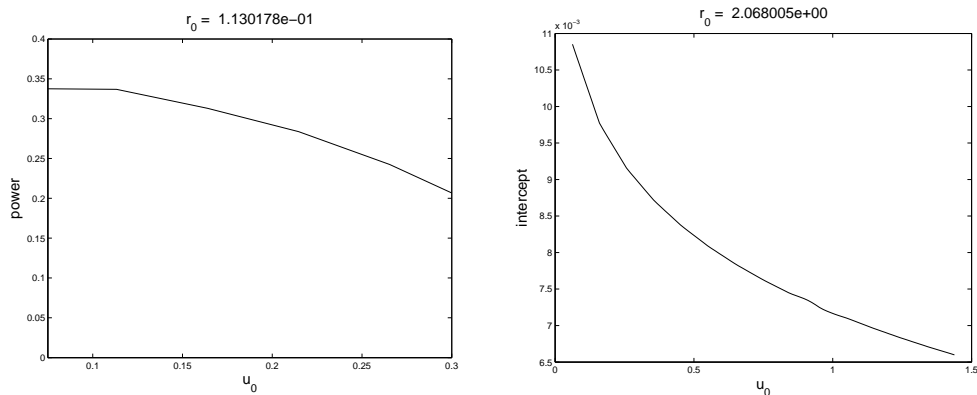


Figure 19: The slope as a function of u_0 with a fixed $r_0 = 0.11302$, with the magnification centered on values of u_0 near 0, and $\alpha \rightarrow 1/3$ (L). The intercept as a function of u_0 with a fixed value of $r_0 = 2.068005$ (R). Again, notice that this is approximately 0.

We first consider $r_0 = 0.11302$ in Figure 18 we see that the slope appears to be quadratic,

and the plot of the power α converges to 2 as u_0 goes to its largest value in the parameter space. As $u_0 \rightarrow 0$, we see $\alpha \rightarrow 1/3$ in Figure 19 (L). For the medium choice of r_0 , we use $r_0 = 2.068005$. The slope appears to be more linear in character, and Figure 20 shows that α is approximately -1 at the upper end of the u_0 values. We see the limit $\alpha \rightarrow 0.45$ as $u_0 \rightarrow 0$ in Figure 21 (L). The third sample is $r_0 = 4.637416$, and we see that the slope is concave down, and indeed, Figure 22 shows the power is between 0.5 and 1 when u_0 is small. The formula for extracting the power is based on logarithms, and does not give reasonable results when $u_0 \approx 1$, thus, as the largest values of u_0 are near 1 for this choice of r_0 , we do not have extracted values for the upper limit here.

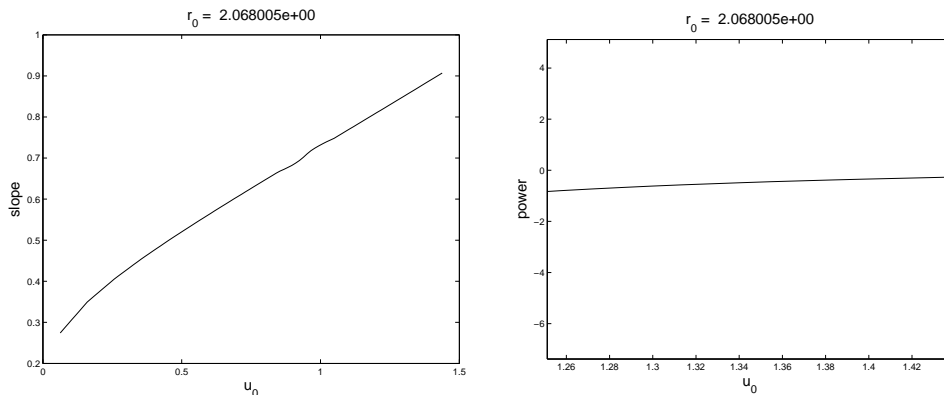


Figure 20: The slope as a function of u_0 with a fixed $r_0 = 2.068005$ (L). A magnified plot of the power α under the assumption that the slope is of the form x^α , with the magnification centered on the largest values of u_0 in this range (R).

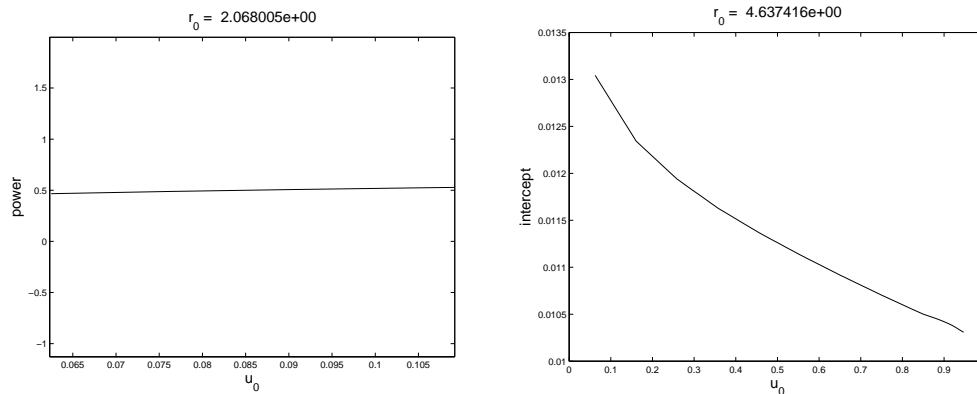


Figure 21: The magnification is centered on values of u_0 near 0, and $\alpha \rightarrow 0.45$ (L). The intercept as a function of u_0 with a fixed value of $r_0 = 4.637416$ (R). Once again, notice that this is approximately 0.

Our final figures are given in order to see how the behavior changes with variable r_0 . In Figure 23 we move r_0 through our range of data from approximately 0 through about 5.5 we

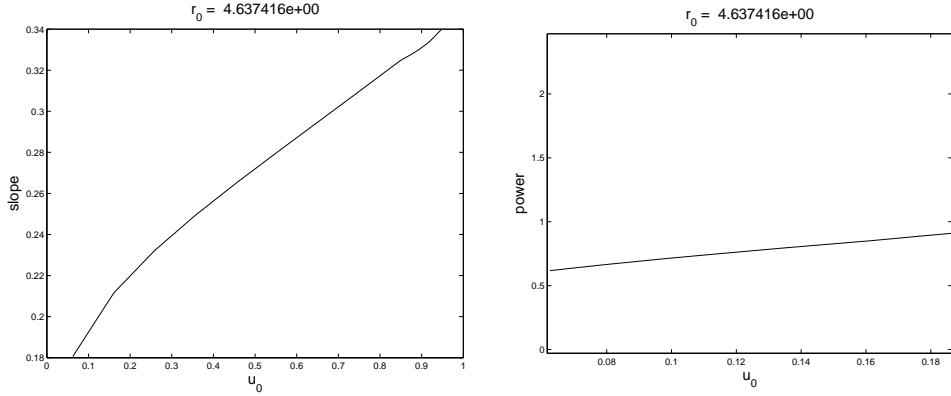


Figure 22: The slope as a function of u_0 with a fixed $r_0 = 4.637416$ (L). A magnified plot of the power α under the assumption that the slope is of the form x^α , with the magnification centered on the largest values of u_0 in this range (R).

take u_0 to be the smallest value in our data set (L), compared to u_0 as the largest value in our data set (R). It is worth mentioning that the plot on the left has a constant u_0 , and the plot on the right has a variable u_0 that is just below the curve f_1 . For small u_0 values (on the left) we see the slope is small, less than 0.4, and decreasing in r_0 . Again, due to the inability to extract the power α when $u_0 \approx 1$, and the shape of the parameter region, we are only able to present the graph of the power as a function of r_0 for the smallest value of u_0 in our data set. This is shown in Figure 24.

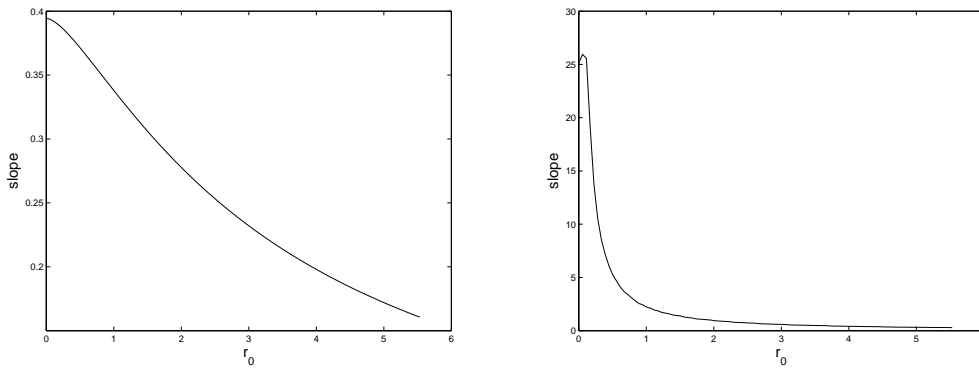


Figure 23: The slope as a function of r_0 with a fixed u_0 with the smallest value we computed (L), and with variable u_0 for the largest value we computed, which is just below f_1 (R).

We summarize our experiments as support for the following conjecture.

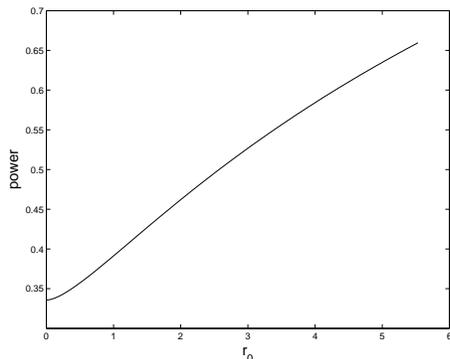


Figure 24: The power α as a function of r_0 with a fixed u_0 value of the smallest we computed.

Conjecture 8.1 *Solutions of the system*

$$\frac{dr}{ds} = \cos \psi \tag{21}$$

$$\frac{du}{ds} = \sin \psi \tag{22}$$

$$\frac{d\psi}{ds} = \kappa u - \frac{\sin \psi}{r} \tag{23}$$

with

$$r(0) = r_0 > 0 \tag{24}$$

$$u(0) = u_0 \tag{25}$$

$$\psi(0) = 0, \tag{26}$$

have linear asymptotes as $s \rightarrow \infty$. The linear asymptotes pass through the origin. Further, the slopes of the linear asymptotes depend on both r_0 and u_0 , and that dependence is approximately quadratic in the initial height u_0 if u_0 is sufficiently far from 0. As $u_0 \rightarrow \infty$, the slope of the asymptote converges to a line with slope u_0^2 . That is, for small r_0 , as $u_0 \rightarrow f_1$, the power α of the slope converges to 2. For u_0 small enough, the slope has the form x^α with α comparable to $1/3$.

References

- [1] Maria Athanassenas, *A free boundary problem for capillary surfaces*, Manuscripta Math. **76** (1992), no. 1, 5–19.
- [2] Paul Concus and Robert Finn, *A singular solution of the capillary equation. I. Existence*, Invent. Math. **29** (1975), no. 2, 143–148.
- [3] ———, *A singular solution of the capillary equation. II. Uniqueness*, Invent. Math. **29** (1975), no. 2, 149–159.
- [4] ———, *The shape of a pendent liquid drop*, Philos. Trans. Roy. Soc. London Ser. A **292** (1978), no. 1391, 307–340.

- [5] Alan Elcrat, Tae-Eun Kim, and Ray Treinen, *Annular capillary surfaces*, Arch. Math. (Basel) **82** (2004), no. 5, 449–467.
- [6] Alan Elcrat, Robert Neel, and David Siegel, *Equilibrium configurations for a floating drop*, J. Math. Fluid Mech. **6** (2004), no. 4, 405–429.
- [7] Alan Elcrat and Ray Treinen, *Numerical results for floating drops*, Discrete Contin. Dyn. Syst. **suppl.** (2005), 241–249.
- [8] Robert Finn, *Equilibrium capillary surfaces*, Grundlehren der Mathematischen Wissenschaften [Fundamental Principles of Mathematical Sciences], vol. 284, Springer-Verlag, New York, 1986.
- [9] ———, *Floating bodies subject to capillary attractions*, J. Math. Fluid Mech. **11** (2009), no. 3, 443–458.
- [10] Robert Finn and Mattie Sloss, *Floating bodies in neutral equilibrium*, J. Math. Fluid Mech. **11** (2009), no. 3, 459–463.
- [11] R. Finn and T. I. Vogel, *On the volume infimum for liquid bridges*, Z. Anal. Anwendungen **11** (1992), no. 1, 3–23.
- [12] Robert Finn and Thomas I. Vogel, *Floating criteria in three dimensions*, Analysis (Munich) **29** (2009), no. 4, 387–402.
- [13] C.F. Gauss, *Principia Generalia Theoriae Figurae Fluidorum*, 1830.
- [14] Enrico Giusti, *Minimal surfaces and functions of bounded variation*, Monographs in Mathematics, vol. 80, Birkhäuser Verlag, Basel, 1984.
- [15] Eduardo H. A. Gonzalez, *Sul problema della goccia appoggiata*, Rend. Sem. Mat. Univ. Padova **55** (1976), 289–302 (Italian).
- [16] James Gordon and David Siegel, *Approximating annular capillary surfaces with equal contact angles*, Pacific J. Math. **247** (2010), no. 2, 371–387.
- [17] ———, *Properties of annular capillary surfaces with equal contact angles*, Pacific J. Math. **247** (2010), no. 2, 353–370.
- [18] W. E. Johnson and L. M. Perko, *Interior and exterior boundary value problems from the theory of the capillary tube*, Arch. Rational Mech. Anal. **29** (1968), 125–143.
- [19] Marquis de La Place, *Celestial mechanics. Vols. I–IV*, Translated from the French, with a commentary, by Nathaniel Bowditch, Chelsea Publishing Co., Inc., Bronx, N.Y., 1966.
- [20] Th. Lohnstein, *Dissertation*, Univ, Berlin, 1891.
- [21] John McCuan, *A variational formula for floating bodies*, Pacific J. Math. **231** (2007), no. 1, 167–191.
- [22] John McCuan and Ray Treinen, *Capillarity and Archimedes’ principle of flotation*, Pacific J. Math. **265** (2013), no. 1, 123–150.
- [23] ———, *On floating equilibria in a finite container*, to appear.
- [24] R. Nickolov, *Uniqueness of the singular solution to the capillary equation*, Indiana Univ. Math. J. **51** (2002), no. 1, 127–169.
- [25] David Siegel, *Height estimates for capillary surfaces*, Pacific J. Math. **88** (1980), no. 2, 471–515.
- [26] ———, *Approximating symmetric capillary surfaces*, Pacific J. Math. **224** (2006), no. 2, 355–365.
- [27] Lloyd N. Trefethen and David Bau III, *Numerical linear algebra*, Society for Industrial and Applied Mathematics (SIAM), Philadelphia, PA, 1997.
- [28] Ray Treinen, *A general existence theorem for symmetric floating drops*, Arch. Math. (Basel) **94** (2010), no. 5, 477–488.
- [29] ———, *Extended annular capillary surfaces*, J. Math. Fluid Mech. **14** (2012), no. 4, 619–632.
- [30] ———, *On the symmetry of solutions to some floating drop problems*, SIAM J. Math. Anal. **44** (2012), no. 6, 3834–3847.

- [31] Bruce Turkington, *Height estimates for exterior problems of capillarity type*, Pacific J. Math. **88** (1980), no. 2, 517–540.
- [32] Thomas I. Vogel, *Symmetric unbounded liquid bridges*, Pacific J. Math. **103** (1982), no. 1, 205–241.
- [33] ———, *Stability of a liquid drop trapped between two parallel planes*, SIAM J. Appl. Math. **47** (1987), no. 3, 516–525.
- [34] Henry C. Wente, *The symmetry of sessile and pendent drops*, Pacific J. Math. **88** (1980), no. 2, 387–397.
- [35] ———, *The stability of the axially symmetric pendent drop*, Pacific J. Math. **88** (1980), no. 2, 421–470.
- [36] T. Young, *An essay on the cohesion of fluids*, Philos. Trans. Roy. Soc. London **96** (1805), 65–87.